International Journal of Bifurcation and Chaos, Vol. 28, No. 6 (2018) 1850072 (20 pages)

DOI: 10.1142/S0218127418500724

Quasi-Periodic Orbits in the Five-Dimensional Nondissipative Lorenz Model: The Role of the Extended Nonlinear Feedback Loop

Sara Faghih-Naini and Bo-Wen Shen*
Department of Mathematics and Statistics,
San Diego State University, 5500 Campanile Drive,
San Diego, CA 92182, USA
*bshen@mail.sdsu.edu

Received ; Revised

A recent study suggested that the nonlinear feedback loop (NFL) of the three-dimensional nondissipative Lorenz model (3D-NLM) serves as a nonlinear restoring force by producing nonlinear oscillatory solutions as well as linear periodic solutions near a nontrivial critical point. This study discusses the role of the extension of the NFL in producing quasi-periodic trajectories using a five-dimensional nondissipative Lorenz model (5D-NLM). An analytical solution to the locally linear 5D-NLM is first obtained to illustrate the association of the extended NFL and two incommensurate frequencies whose ratio is irrational, yielding a quasi-periodic solution. The quasi-periodic solution trajectory moves endlessly on a torus but never intersects itself.

While the NFL of the 3D-NLM consists of a pair of downscaling and upscaling processes, the extended NFL within the 5D-NLM additionally introduces two new pairs of downscaling and upscaling processes that are enabled by two high wavenumber modes. One pair of downscaling and upscaling processes provides a two-way interaction between the original (primary) Fourier modes of the 3D-NLM and the newly-added (secondary) Fourier modes of the 5D-NLM. The other pair of downscaling and upscaling processes involves interactions amongst the secondary modes. By comparing the numerical simulations using one- and two-way interactions, we illustrate that the two-way interaction is crucial for producing the quasi-periodic solution. A follow-up study using a 7D nondissipative LM shows that a further extension of NFL, which may appear throughout the spatial mode-mode interactions rooted in the nonlinear temperature advection, is capable of producing one more incommensurate frequency.

Keywords: Nondissipative Lorenz model; nonlinear feedback loop; quasi-periodicity.

1. Introduction

Over 50 years ago, Lorenz [1963] proposed an elegant set of three nonlinear ordinary differential equations to illustrate the sensitive dependence of solutions on initial conditions (ICs) and challenged views on (long-term) deterministic predictability. His simple but high-impact nonlinear model is called the Lorenz model (LM) and, in this study, is referred to as the three-dimensional LM (3DLM). Sensitive dependence on ICs, which is known as the butterfly effect of the first kind, suggests a finite predictability for weather and climate (e.g. [Solomon *et al.*, 2007; Anthes, 2011]). An inferred view that small scale processes may significantly alter large-scale processes is also known as the butterfly effect but is referred to as the second kind of butterfly effect (e.g. [Shen, 2014, 2015, 2016, 2017~~a~~; Shen *et al.*, 2018]). As a result of its profound importance, the 3DLM has been extensively studied and related research has further inspired many studies dealing with nonlinear dynamics (e.g. [Gleick, 1987; Sprott, 2003; Jordan & Smith, 2007; Hirsch *et al.*, 2013; Strogatz, 2015]).

While the 3DLM clearly demonstrates solution dependence on ICs for chaotic solutions, high-dimensional LMs have been derived for understanding the impact of mode truncations on solution stability and the route to chaos (e.g. [Curry, 1978; Curry *et al.*, 1984; Howard & Krishnamurti, 1986; Hermiz *et al.*, 1995; Thiffeault & Horton, 1996; Musielak *et al.*, 2005; Roy & Musielak, 2007a, 2007b, 2007c]). In our recent studies using high-dimensional LMs (e.g. [Shen, 2014, 2015, 2016]), we selected new modes in order to extend the nonlinear feedback loop that is capable of providing additional nonlinear feedback for stabilizing or destabilizing solutions. The 3DLM and 5DLM, as well as other high-dimensional Lorenz models, were derived from the Rayleigh–Benard convection equations that include three types of physical processes including heating, dissipative, and nonlinear advection (e.g. [Saltzman, 1962; Lorenz, 1963]). The nonlinear feedback loop of the 3DLM consists of a pair of downscaling and upscaling processes that describe temperature advection by various (spatial) Fourier modes. Mathematically, these processes are represented by the nonlinear terms $-XZ$ and XY in the 3DLM [e.g. Eqs. (2) and (3)], respectively. The 5DLM has two additional (spatial) Fourier modes that have high wavenumbers. These newly-added high wavenumber modes are referred to as secondary (spatial) modes, while the fundamental Fourier modes in the original 3DLM are referred to as primary modes. The ratio for wavenumbers in the primary and secondary modes is rational.

Our approach, using incremental changes in the number of Fourier modes, was to help trace the collective impact of additional linear and nonlinear terms on solution stability as well as the extension of the nonlinear feedback loop. With the proper selection of modes, the five-dimensional LM (5DLM, [Shen, 2014]) and the seven-dimensional LM (7DLM, [Shen, 2016]) have larger critical values, as compared to the 3DLM, for the normalized Rayleigh parameter for the onset of chaos. Critical values for the Rayleigh parameter in the 3DLM, 5DLM, and 7DLM are 24.74, 42.9, and 116.9, respectively. The studies above suggest that system stability for LMs with a finite number of modes can be improved using additional high wavenumber modes that provide a negative nonlinear feedback associated with additional dissipative terms. In contrast, as shown by comparing the six-dimensional LM (6DLM) with the 5DLM [Shen, 2015] as well as by comparing the nine-dimensional LM (9DLM) with the 7DLM [Shen, 2017~~a~~], positive nonlinear feedback associated with an additional heating term may destabilize solutions. Due to these findings, we have focused on the addition of high wavenumber modes for extending the nonlinear feedback such that the negative feedback is stronger than the positive feedback. Recently, Moon *et al.* [2017] discussed the dependence of solutions on a wide range of system parameters within the 5DLM, 6DLM and higher-dimensional Lorenz models. Felício and Rech [2018] conducted a comprehensive analysis on the shape of bifurcation diagrams, periodic, and chaotic attractors within the 5DLM and 6DLM, showing hyperchaos in the 6DLM.

Since studies using the 3DLM began, nonlinearity has been viewed as the source of chaos in the 3DLM. Some researchers have further inferred that systems containing more nonlinear terms may become more chaotic. On the other hand, by using the 5DLM and 7DLM we have shown that the collective impact of increased degrees of nonlinearity and additional dissipative terms provides negative feedback for stabilizing solutions. The impact of an increased degree of nonlinearity on the solution can be further examined in a nondissipative system (i.e. with no dissipation), a simpler system with only heating and nonlinear terms. Using the 3D nondissipative LM (3D-NLM), we found that the nonlinear feedback loop of the 3D-NLM serves as a nonlinear restoring force by producing nonlinear oscillatory solutions [Shen, ~~2017b~~] as well as linear periodic solutions near a nontrivial critical point. We additionally discussed how heating and the nonlinear feedback loop may collectively produce a periodic solution.

From the perspective of numerical weather prediction, our ultimate goal is to apply numerical results obtained using idealized LMs in order to improve our understanding of predictability in real-world weather/climate models [Shen *et al.*, 2006; Shen *et al.*, 2010~~a~~; Shen *et al.*, 2013]. Specifically, it is important to understand if and how increased resolutions in weather/climate models can suppress or enhance chaotic responses because high-resolution global modeling, the current trend, requires tremendous computing resources. Therefore, we extend the study with the 3D-NLM to the 5D-NLM.

In addition to periodic solutions, quasi-periodic solutions may appear in conservative systems. When a system has two (or more) components with different frequencies whose ratio is irrational, composite motion with two (or more) components is called quasi-periodic and the frequencies are called incommensurate. A quasi-periodic solution moves endlessly on a torus but never intersects itself. The orbit is never closed, so it is not periodic. However, as a result of arbitrarily close repetition, the motion is also said to be recurrent and its orbit is dense on the torus (e.g. [Thompson & Stewart, 2002]). Since two distinct frequencies are required, a quasi-periodic solution may appear in a two-dimensional system with an external periodic forcing or in a higher-dimensional (autonomous) system.

While the nonlinear feedback loop of the 3D-NLM can produce periodic solutions, in this study, we show that the extension of the nonlinear feedback loop is critical for producing a quasi-periodic solution in the 5D-NLM. The paper is organized as follows: In Sec. 2, we discuss the governing equations of the 5D-NLM and the analytical and numerical methods. In Sec. 3, we present analytical solutions to illustrate two incommensurate frequencies that lead to a quasi-periodic solution. We illustrate the role of the extended nonlinear feedback loop in producing incommensurate frequencies using eigenvalue analysis and numerical simulations. We additionally discuss numerical experiments that we design for examining the impact of the two coupling terms (that provide two-way interactions between the primary and secondary modes) on the quasi-periodicity of solutions. Concluding remarks are provided at the end. In Appendix A, we apply the same methods to the 3D-NLM and compare our results using a recent study by [Shen, ~~2017b~~], for verification. Appendix B presents detailed derivations for the analytical solution in the locally linear 5D-NLM. Appendix C provides an analogy between the locally linear 5D-NLM and a coupled spring system [Fay & Graham, 2003].

2. The Five-Dimensional Nondissipative Lorenz Model (5D-NLM)

In this section, we present equations for the 5D-NLM and discuss analytical and numerical methods for obtaining and analyzing solutions. The 5D-NLM can be obtained by ignoring the dissipative terms from the 5DLM [Shen, 2014], as follows:

$$\frac{dX}{d\tau} = \cancel{-\sigma X} + \sigma Y, \tag{1}$$

$$\frac{dY}{d\tau} = -XZ + rX \cancel{- Y}, \tag{2}$$

$$\frac{dZ}{d\tau} = XY - XY_1 \cancel{- bZ}, \tag{3}$$

$$\frac{dY_1}{d\tau} = XZ - 2XZ_1 \cancel{- d_0 Y_1}, \tag{4}$$

$$\frac{dZ_1}{d\tau} = 2XY_1 \cancel{- 4bZ_1}. \tag{5}$$

A crossout symbol is applied to each of the dissipative terms that are neglected in the 5D-NLM. As discussed in [Shen, 2014], (X, Y, Z, Y_1, Z_1) represent the amplitude of the Fourier modes. (X, Y, Z), which appear in the 3DLM, are referred to as the primary modes. (Y_1, Z_1), which are included as high wavenumber modes in the 5DLM, are referred to as the secondary modes. τ is dimensionless time. σ is the Prandtl number, and r is the normalized Rayleigh number or the heating parameter. Detailed information regarding these parameters is provided in [Shen, 2014]. The "forcing" terms on the right-hand side of the above equations are referred to as the linear force (or the linear heating term, rX) and the nonlinear force terms (e.g. $-XZ$ and XY). Shen [2014] showed that the nonlinear terms $-XZ$ and XY form a nonlinear feedback loop with a pair of upscaling and downscaling processes amongst the primary modes (e.g. Y and Z). With inclusion of secondary modes, two additional pairs of upscaling and downscaling processes are introduced. One pair contains $-XY_1$ and XZ and the other pair includes $-2XZ_1$ and $2XY_1$. The former enables two-way interactions between the primary and secondary modes. The latter indicates two-way interactions amongst the secondary modes. The nonlinear terms $-XY_1$ and XZ are also referred to as coupling terms due to their role in coupling the primary and secondary modes. The two additional pairs of upscaling and downscaling processes extend the original nonlinear feedback loop with $-XZ$ and XY.

In this study, we discuss the appearance of a quasi-periodic solution that is associated with the extended nonlinear feedback loop. To achieve our goal, we apply a perturbation method for transforming the above equations into a system that could help us investigate linear or nonlinear numerical solutions. For each of the above variables, we decompose a total field (e.g. U) into the reference (or basic) state U_c and a perturbation U' (i.e. $U = U_c + U'$). Here, a variable with a subscript c indicates a reference (or basic) state and a variable with a prime represents a perturbation. In this study, we use a nontrivial critical point solution as the reference state. Applying the perturbation method to Eqs. (1)–(5) produces the following equations:

$$\frac{dX'}{d\tau} = \sigma Y', \tag{6}$$

$$\frac{dY'}{d\tau} = (r - Z_c)X' - X_cZ' - FN(X'Z'), \tag{7}$$

$$\frac{dZ'}{d\tau} = (Y_c - Y_{1c})X' + X_cY' - X_cY'_1 + FN(X'Y' - X'Y'_1), \tag{8}$$

$$\frac{dY'_1}{d\tau} = (Z_c - 2Z_{1c})X' + X_cZ' - 2X_cZ'_1 + FN(X'Z' - 2X'Z'_1), \tag{9}$$

$$\frac{dZ'_1}{d\tau} = 2Y_{1c}X' + 2X_cY'_1 + 2FN(X'Y'_1). \tag{10}$$

Here, a "flag" FN is introduced. Equations (6)–(10) with $FN = 1$ are identical to Eqs. (1)–(5) while Eqs. (6)–(10) with $FN = 0$ represent a locally linear system with respect to the basic state. Therefore, Eqs. (6)–(10) can be used to obtain linear ($FN = 0$) and nonlinear ($FN = 1$) numerical solutions. To facilitate discussions, Eqs. (1)–(5) are referred to as the 5D-NLM V1 while Eqs. (6)–(10) are referred to as the 5D-NLM V2. As compared to the 3DLM, the 5D-NLM V2 (with $FN = 0$ or $FN = 1$) contains an increased degree of nonlinearity (e.g. $X_cY'_1$) that is based on "nonlinear" interactions between the primary and secondary Fourier modes through the Jacobian term that represents the nonlinear advection of potential temperature [e.g. Eq. (2) of [Shen, 2014]]. Mathematically, multiplication of two spatial modes with different wavenumbers in the Jacobian term may produce a third mode whose wavenumber is different from those of the original two modes. Both the 5D-NLM V1 [i.e. Eqs. (1)–(5)] and V2 [i.e. Eqs. (6)–(10)] include the extension of the nonlinear feedback loop (via spatial mode-mode interaction). While the 5D-NLM V1 describes the evolution of the amplitude for each of the Fourier modes, the V2 [i.e. Eqs. (6)–(10)] depicts the evolution of the amplitude's departures (i.e. perturbations) from the time-independent reference state. Comparing both the 5D-NLM [Eqs. (6)–(10)] and 3D-NLM [Eqs. (A.1)–(A.3) in Appendix A] with $FN = 0$, the two terms highlighted in circles (i.e. $-X_cY'_1$ and X_cZ') are the coupling terms. The coupling terms introduced by inclusion of the secondary modes (i.e. Y_1 and Z_1) extend the nonlinear feedback loop. In other words, Eqs. (6)–(8) (with $FN = 0$) can be viewed as an extension of the 3D-NLM (with $FN = 0$) that includes the feedback term $-X_cY'_1$ from the secondary mode. Furthermore, when the term $-X_cY'_1$ is neglected, Eqs. (6)–(8) (with $FN = 0$) are reduced to become 3D-NLM (with $FN = 0$).

To assure the validity of our numerical approaches, we present analytical and numerical solutions for the locally linear and nonlinear 3D-NLM in Appendix A. The same numerical approaches are applied to perform simulations with the 5D-NLM V2. To illustrate the quasi-periodic solution, we first solve the locally linear system (i.e. the 5D-NLM V2 with $FN = 0$) to obtain the analytical solutions of eigenvalues and eigenvectors. The eigenvalues are used to indicate the appearance of incommensurate frequencies and the eigenvectors, as well as eigenvalues, are used to construct an analytical solution for the quasi-periodic orbit. By performing numerical simulations, we then discuss the impact of the extended nonlinear feedback loop (and the coupling terms as well) on the appearance of quasi-periodic solutions.

2.1. *Analytical and numerical methods*

Analyzing the 5D-NLM V1 (or V2), we can choose the following basic (or reference) state: $(Y_c, Z_c, Y_{1c}, Z_{1c}) = (0, r, 0, \frac{r}{2})$, X_c can be any number and, to facilitate discussions, is assumed to be positive.

With the choice of the basic state, the locally linear system can be expressed as follows:

$$\frac{d\overrightarrow{U'}}{d\tau} = A^{5D}\overrightarrow{U'}, \tag{11}$$

where $\overrightarrow{U'}$ is a column vector and its transpose is equal to (X', Y', Z', Y_1', Z_1'), and

$$A^{5D} = \begin{pmatrix} 0 & \sigma & 0 & 0 & 0 \\ 0 & 0 & -X_c & 0 & 0 \\ 0 & X_c & 0 & -X_c & 0 \\ 0 & 0 & X_c & 0 & -2X_c \\ 0 & 0 & 0 & 2X_c & 0 \end{pmatrix}. \tag{12}$$

We first solve the analytical solutions of the eigenvalues and eigenvectors using the above matrix and apply them to obtain an analytical solution. An eigenvalue (λ) and its corresponding eigenvector ($\overrightarrow{V}$) are determined by the relationship $A^{5D}\overrightarrow{V} = \lambda\overrightarrow{V}$. To examine the validity of the method, we apply it for solving the 3D-NLM and discuss the results in Appendix A. Here, it should be noted that the upper box in Eq. (12) represents the matrix of the 3D-NLM [e.g. Eq. (A.5)]. In Sec. 3.1, we discuss solutions for the eigenvalues and eigenvectors of the matrix for the 5D-NLM.

For numerical solutions of the 5D-NLM V2 (or V1), the solver of ordinary differential equations in Python is used to perform numerical simulations. Without a loss of generality, parameters, including $r = 25$ and $\sigma = 10$, are kept constant. A dimensionless time interval ($\triangle\tau$) of 0.001 is used and the total number of time steps is 2,048, giving a total dimensionless time (τ) of 2.048. We select the parameters in order to analyze the spectrum using a FFT (Fast Fourier Transform) and to illustrate the periodicity of solutions. Longer time simulations are also performed to confirm our conclusions. In this study, the initial conditions (ICs) for the control run are the following:

$$(X, Y, Z, Y_1, Z_1) = (X_o, 0, 0, 0, 0), \tag{13a}$$

which yields:

$$(X', Y', Z', Y_1', Z_1') = \left(X_o - X_c, 0, -r, 0, -\frac{r}{2}\right). \tag{13b}$$

Since our focus is illustrating the role of the extended nonlinear feedback loop in producing quasi-periodic solutions, without a loss of generality, the reference (basic) state X_c is determined as described in the following discussion. Using Eqs. (1), (3), and (5), we can obtain the following conservation law (e.g. [Shen, 2014]):

$$\frac{X^2}{2} - \sigma\left(Z + \frac{Z_1}{2}\right) = \text{constant} = \frac{X_o^2}{2}, \tag{14}$$

which represents conservation of the normalized total energy (i.e. the sum of kinetic and potential energies). In the 3D-NLM, the conservative quantity, one of the so-called Nambu Hamiltonians (e.g. [Nambu, 1973; Nevir & Blender, 1994; Floratos, ~~2011~~; Roupas, 2012; Blender & Lucarini, 2013]), becomes $X^2/2 - \sigma Z = $ constant. After plugging $Z_c = r$ and $Z_{1c} = r/2$ into the above equation, X_c is determined as:

$$X_c = \sqrt{X_o^2 + \frac{5\sigma r}{2}}. \tag{15}$$

The second term inside the radical sign, $5\sigma r/2$, is denoted by X^2_{cntl} (i.e. $X_{\text{cntl}} = \pm\sqrt{5\sigma r/2}$). To simplify discussions, we assume a positive X_{cntl} and use $X_o = X_{\text{cntl}}$ as the initial condition of the control run. In the three parallel runs, the ICs for X_o are given by $0.25X_{\text{cntl}}$, $0.5X_{\text{cntl}}$ and $4X_{\text{cntl}}$, respectively. While perturbations are computed analytically or numerically using the 5D-NLM V2 with $FN = 0$ or $FN = 1$, the total fields shown in the figures are discussed in the next section. A frequency analysis is performed using perturbations. Since Y_c and Y_{1c} are zero, Y' and Y_1' also represent the total fields. To assure the validity of our approaches, solutions for both 5D-NLM V1 and V2 that are identical are compared (not shown).

3. Results and Discussions

3.1. *Linear analytical solutions*

Assuming $i\beta$ to be an eigenvalue of the matrix in Eq. (12), the characteristic equation of the locally linear system is given by:

$$\det\begin{pmatrix} -i\beta & \sigma & 0 & 0 & 0 \\ 0 & -i\beta & -X_c & 0 & 0 \\ 0 & X_c & -i\beta & -X_c & 0 \\ 0 & 0 & X_c & -i\beta & -2X_c \\ 0 & 0 & 0 & 2X_c & -i\beta \end{pmatrix} = 0, \tag{16a}$$

which is equivalent to:

$$\beta(\beta^4 - 6\beta^2 X_c^2 + 4X_c^4) = 0. \tag{16b}$$

The above yields the following solutions:

$$\begin{aligned}
\beta_1 &= \sqrt{(3+\sqrt{5})X_c},\\
\beta_2 &= -\sqrt{(3+\sqrt{5})X_c},\\
\beta_3 &= \sqrt{(3-\sqrt{5})X_c},\\
\beta_4 &= -\sqrt{(3-\sqrt{5})X_c} \quad \text{and}\\
\beta_5 &= 0.
\end{aligned} \tag{17}$$

Here, real numbers β_1–β_4 indicate two pairs of imaginary eigenvalues for the matrix. The eigenvectors corresponding to the eigenvalues $i\beta_1$–$i\beta_5$ are:

$$\vec{V_k} = \begin{pmatrix} X' \\ Y' \\ Z' \\ Y_1' \\ Z_1' \end{pmatrix} = \begin{pmatrix} \sigma\left(\dfrac{-\beta_k^2}{2X_c^3} + \dfrac{5}{2X_c}\right) \\ i\beta_k\left(\dfrac{-\beta_k^2}{2X_c^3} + \dfrac{5}{2X_c}\right) \\ \dfrac{-\beta_k^2}{2X_c^2} + 2 \\ \dfrac{i\beta_k}{2X_c} \\ 1 \end{pmatrix},$$

here $k = 1, 2, 3, 4$ and

$$\vec{V_5} = \begin{pmatrix} \sigma \\ 0 \\ 0 \\ 0 \\ 0 \end{pmatrix}. \tag{18}$$

For each of the eigenvectors corresponding to β_1–β_4, the ratio (R_y) between the second and fourth components (rows) is:

$$R_y(\beta_k) = 2X_c\left(\frac{-\beta_k^2}{2X_c^3} + \frac{5}{2X_c}\right) = \frac{1}{X_c^2}(5X_c^2 - \beta_k^2), \tag{19a}$$

yielding:

$$\begin{aligned}
&R_y(\beta_k) < 0 \quad \text{for } \beta_1 \text{ and } \beta_2 \text{ and}\\
&R_y(\beta_k) > 0 \quad \text{for } \beta_3 \text{ and } \beta_4.
\end{aligned} \tag{19b}$$

Similarly, the ratio (R_z) between the third and fifth components (rows) is:

$$R_z(\beta_k) = \frac{-\beta_k^2}{2X_c^2} + 2 = \frac{1}{2X_c^2}(4X_c^2 - \beta_k^2), \tag{20a}$$

leading to:

$$\begin{aligned}
&R_z(\beta_k) < 0 \quad \text{for } \beta_1 \text{ and } \beta_2 \text{ and}\\
&R_z(\beta_k) > 0 \quad \text{for } \beta_3 \text{ and } \beta_4.
\end{aligned} \tag{20b}$$

Physical interpretations in Eqs. (19b) and (20b) are provided below in Fig. 1. Using the eigenvalues and eigenvectors [e.g. Eqs. (17) and (18)], a general

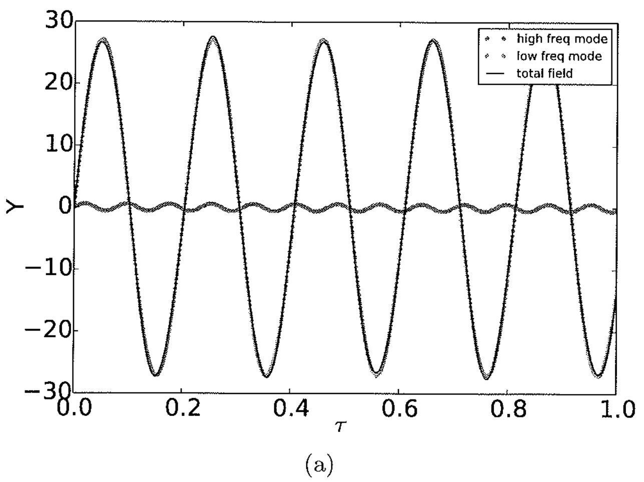

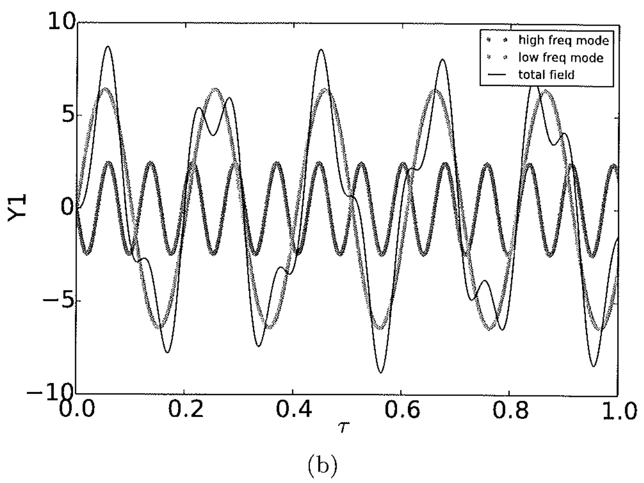

Fig. 1. An analytical solution of the locally linear 5D-NLM for time evolution of the primary and secondary modes (i.e. Y and Y_1) for $\tau \in [0, 2.048]$ [i.e. Eq. (22)]. The total field for Y in (a) and for Y_1 in (b). High-frequency components for Y and Y_1 in (c), which are out of phase. Low-frequency components for Y and Y_1 in (d), which are in phase. Solid lines indicate the primary mode (Y). Dashed lines indicate the secondary mode (Y_1).

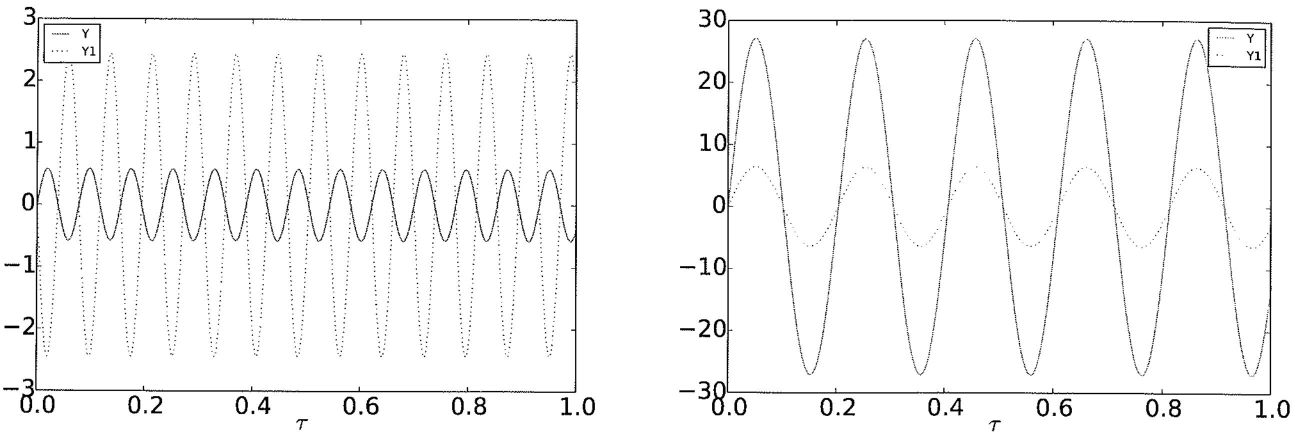

(c)

(d)

Fig. 1. (*Continued*)

solution, denoted by $\overrightarrow{U'}$ with its transpose of (X', Y', Z', Y_1', Z_1'), can be written as follows:

$$\overrightarrow{U'}(\tau) = C_1 e^{i\beta_1\tau}\overrightarrow{V_1} + C_2 e^{i\beta_2\tau}\overrightarrow{V_2} + C_3 e^{i\beta_3\tau}\overrightarrow{V_3} + C_4 e^{i\beta_4\tau}\overrightarrow{V_4} + C_5 e^{i\beta_5\tau}\overrightarrow{V_5}, \tag{21}$$

where C_1–C_5 are constant coefficients that can be determined by a specific IC. The above time dependent solution consists of trigonometric functions with frequencies of β_j. Two different frequencies are β_1 and β_3. Since the ratio of β_1 and β_3 is irrational, the two frequencies are incommensurate. Therefore, a quasi-periodic solution with a dense orbit on a torus is expected, as discussed below.

For the given IC in Eq. (13b), the corresponding solution becomes:

$$\begin{pmatrix} X' \\ Y' \\ Z' \\ Y_1' \\ Z_1' \end{pmatrix} = \frac{-\beta_3^2 r}{2(\beta_3^2-\beta_1^2)} \begin{pmatrix} \sigma\left(\dfrac{-\beta_1^2}{2X_c^3} + \dfrac{5}{2X_c}\right)\cos(\beta_1\tau) \\ -\beta_1\left(\dfrac{-\beta_1^2}{2X_c^3} + \dfrac{5}{2X_c}\right)\sin(\beta_1\tau) \\ \left(\dfrac{-\beta_1^2}{2X_c^2} + 2\right)\cos(\beta_1\tau) \\ \dfrac{-\beta_1}{2X_c}\sin(\beta_1\tau) \\ \cos(\beta_1\tau) \end{pmatrix} + \frac{\beta_1^2 r}{2(\beta_3^2-\beta_1^2)} \begin{pmatrix} \sigma\left(\dfrac{-\beta_3^2}{2X_c^3} + \dfrac{5}{2X_c}\right)\cos(\beta_3\tau) \\ -\beta_3\left(\dfrac{-\beta_3^2}{2X_c^3} + \dfrac{5}{2X_c}\right)\sin(\beta_3\tau) \\ \left(\dfrac{-\beta_3^2}{2X_c^2} + 2\right)\cos(\beta_3\tau) \\ \dfrac{-\beta_3}{2X_c}\sin(\beta_3\tau) \\ \cos(\beta_3\tau) \end{pmatrix}$$
$$+ \left(\frac{X_0 - X_c}{\sigma} + \frac{5r}{4X_c}\right)\begin{pmatrix} \sigma \\ 0 \\ 0 \\ 0 \\ 0 \end{pmatrix}. \tag{22}$$

Appendix B provides detailed procedures for determining the coefficients C_1–C_5. From Eq. (22), each of the perturbation variables can be expressed as a linear combination of three eigenmodes in big brackets on the right-hand side. The first two eigenmodes are oscillatory, have frequencies of β_1 and β_3, and are referred to as high- and low-frequency eigenmodes (or components), respectively. The third mode is nonoscillatory.

With the exception of X', the projections of the other perturbation variables onto the third nonoscillatory eigenmode are zero. As shown in Eq. (19), the ratio of Y' and Y'_1 that are projected onto the high-frequency component (i.e. β_1) is negative. Therefore, they are out of phase. In contrast, for the low-frequency component (i.e. β_3), the projections of Y' and Y'_1 are in phase because their ratio is positive [e.g. Eq. (19)]. In a similar manner, projections of Z' and Z'_1 onto the high-frequency component are out of phase and their projections onto the low-frequency component are in phase [e.g. Eq. (20)].

Before we discuss the analytical and numerical solutions of the 5D NLM V2, we draw the reader's attention to the following terms: spatial Fourier modes and temporal high- and low-frequency components (or eigenmodes). As shown in Eq. (22), the solutions include amplitudes of Fourier modes at different spatial scales (e.g. Y and Y_1); and the amplitude of a specific spatial mode (e.g. Y) may have different temporal frequencies (e.g. β_1 and β_3). Each of the periodic components for the solutions of Y' and Y'_1 in Eq. (22), as well as their sums, are displayed in Figs. 1(a) and 1(b). Note that as Y_c and Y_{1c} are zero, the solutions in Fig. 1 also represent the total fields. Interestingly, the amplitude of the high-frequency component for Y' is much smaller than that of the low-frequency component, as explained below. For the primary mode (Y') in Eq. (22), the ratio of the amplitude of the high-frequency component to that of the low-frequency component is

$$\frac{-\beta_3}{\beta_1}\left(\frac{5X_c^2-\beta_1^2}{5X_c^2-\beta_3^2}\right) = (9-4\sqrt{5})\frac{\beta_3}{\beta_1} \approx 0.056\frac{\beta_3}{\beta_1},$$

which is small. Therefore, the total solution of the primary mode Y' is dominated by the low-frequency component. In contrast, for the secondary mode Y'_1, the ratio of the amplitude of the high-frequency component to that of the low-frequency component is β_3/β_1, which is about 0.38. The result suggests that both high-frequency and low-frequency components contribute to the secondary mode Y'_1. Given a specific temporal frequency (e.g. β_1 or β_3), Fig. 1(c) [1(d)] indicates that the components of Y' and Y'_1 at the high (low) frequency are out of phase (in phase), consistent with the analysis using Eq. (19b) [(20b)]. The spectrum of the analytical solution for Y' (Y'_1) using Eq. (22) is provided in Fig. 2 and clearly shows two peaks at distinct frequencies. The locations of the peaks are the same as those obtained from the eigenvalue analysis using Eq. (17). The spectral analysis is applied in order to compare the spectrum of linear and nonlinear numerical solutions.

Figure 3 displays the X–Y, X–Z, Y–Y_1, and Y_1–Z_1 plots. Compared to periodic solutions of the 3D-NLM (e.g. Fig. 8), these solution orbits are not closed. The recurrent trajectories are confined within a region. The size of the region where a trajectory travels is determined by the (relative) magnitudes of the corresponding components (e.g. X and Y) and by the relative magnitudes of the

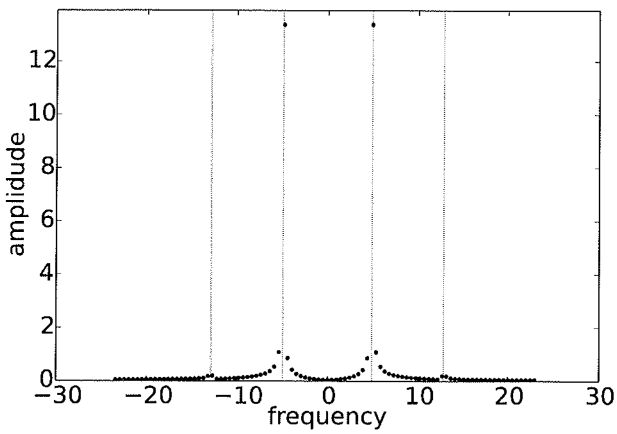

(a)

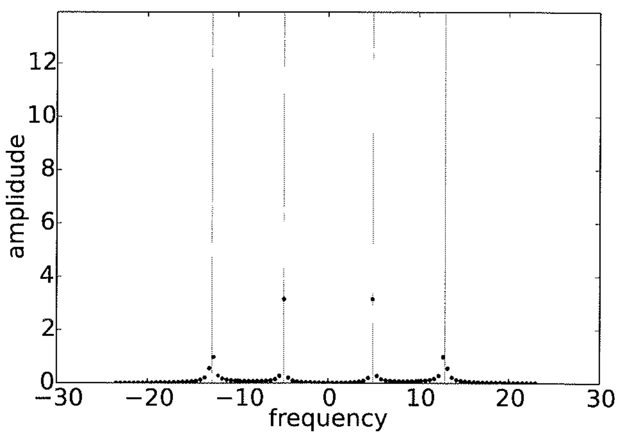

(b)

Fig. 2. A frequency analysis displaying the amplitudes of Y and Y_1 at different frequencies (i.e. the square root of the spectra) from the analytical solution in Eq. (22) for $\tau \in [0, 2.048]$. The vertical lines in blue and red indicate the frequencies obtained from the analytical solution of eigenvalues as reference lines for a comparison with the numerical simulations. Spectrum of the total: (a) Y and (b) Y_1.

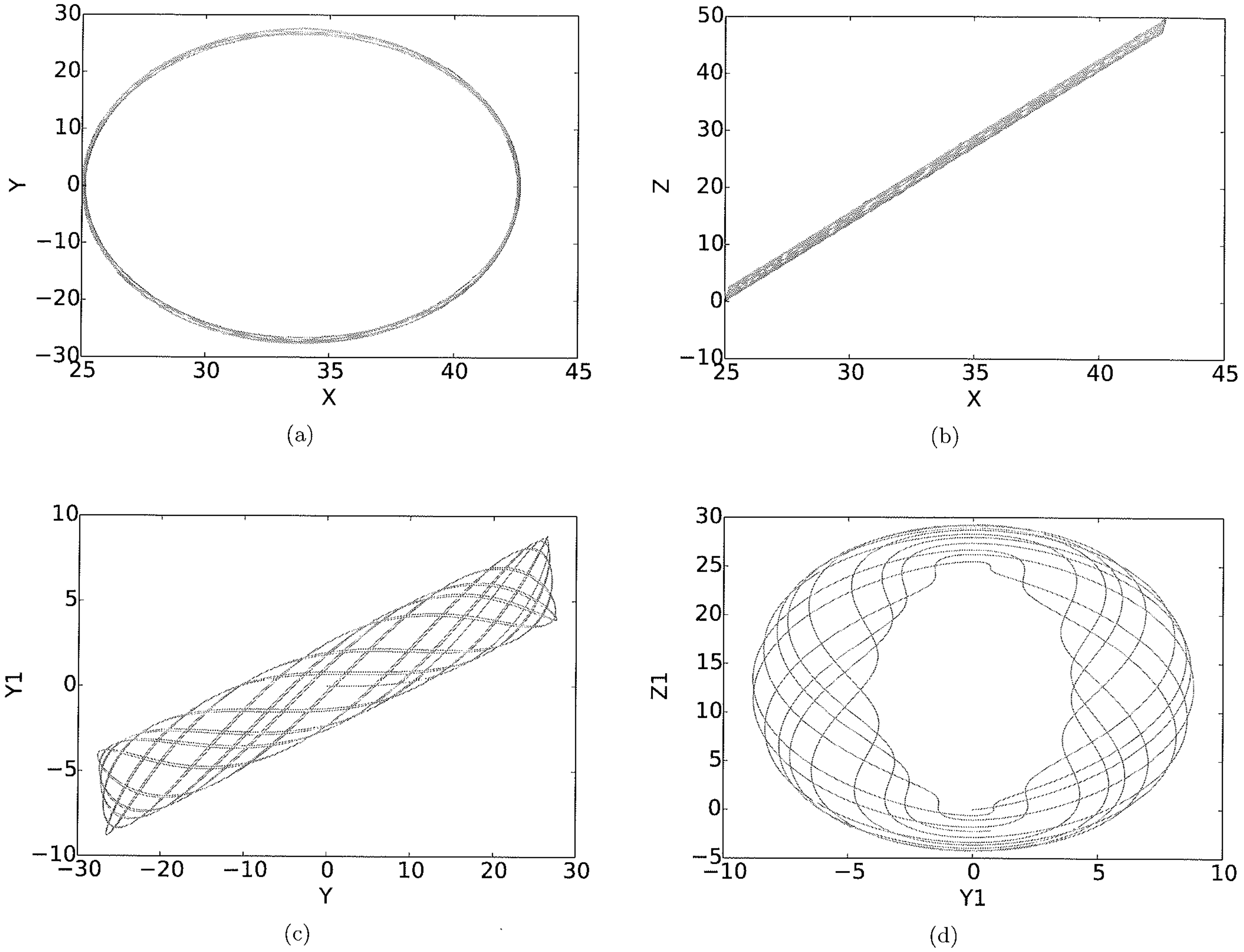

Fig. 3. Analytical solutions for various modes in the 5D-NLM V2 for $\tau \in [0, 2.048]$. (a) X–Y, (b) X–Z, (c) Y–Y_1 and (d) Y_1–Z_1.

low- and high-frequency components [in Fig. 3(a)]. Since the low-frequency component plays a dominant role in solutions for the primary modes (e.g. Y) (i.e. its high-frequency component is relatively insignificant), the areas of the recurrent trajectories appear as bicycle tubes. Note that the orbits are not closed but are quasi-periodic. By comparison, since both low- and high-frequency components are important in the secondary modes, quasi-periodicity is best shown using solutions for the secondary modes [e.g. Fig. 3(c) or 3(d)].

3.2. *Linear and nonlinear numerical solutions*

As discussed in [Shen, ~~2017b~~], the original nonlinear feedback loop of the 3D-NLM acts as a (nonlinear) restoring force to produce (linear and nonlinear) periodic solutions (as well as the so-called homoclinic orbit solution). In the previous section, we discussed the analytical solutions and the corresponding frequencies in order to illustrate the quasi-periodicity using the locally linear 5D-NLM V2 which consists of Eqs. (6)–(10) with $FN = 0$. Here, we examine the association of the quasi-periodic solutions with the extended nonlinear feedback loop using numerical simulations produced by the 5D-NLM V2. We first compare analytical and numerical solutions of the 5D-NLM V2 with $FN = 0$ as model verification. Then, the model with $FN = 0$ and $FN = 1$ is used for comparing linear and nonlinear simulations in order to reveal the impact of nonlinearity on the quasi-periodicity of solutions.

Figures 4(a)–4(c) provide a time evolution of the analytical solutions and linear simulations with $FN = 0$ in the 5D-NLM V2. As shown with X,

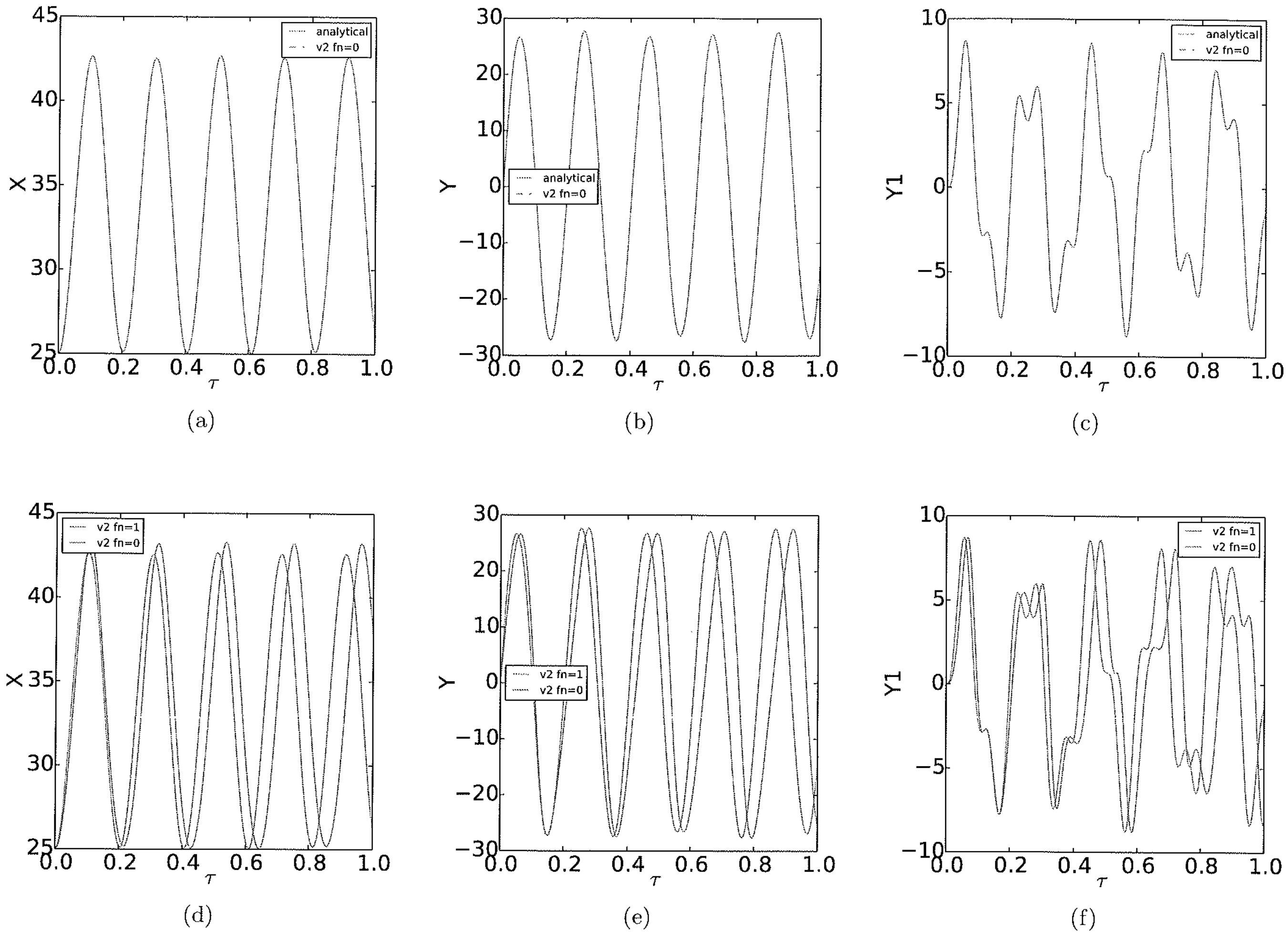

Fig. 4. A time evolution of X, Y and Y_1. (a)–(c) A comparison of the analytical solutions in Eq. (22) and numerical results from the 5D-NLM V2 with $FN = 0$. (d)–(f) A comparison of linear and nonlinear simulations with $FN = 0$ and $FN = 1$ in the 5D-NLM V2.

Y, and Y_1, good agreement between the analytical and numerical solutions is obtained. By choosing $FN = 1$ and repeating the numerical simulations, the impact of nonlinearity on the solutions is examined. As shown in Figs. 4(d)–4(f), the nonlinear simulations produce larger amplitudes and larger periods as compared to the linear simulations. Overall, the nonlinear solution has two dominant frequencies. The underlying mechanism for the nonlinear modulation in producing a larger period for the case with a relatively small X_o is beyond the scope of this study. Instead, as discussed using Figs. 5 and 6, we compare cases with a small and large X_o to illustrate the initial conditions under which a (linear) quasi-periodic solution may capture the major feature of the corresponding nonlinear solution.

In addition to the control run, parallel experiments are performed by varying X_o in order to understand the dependence of solutions on the ICs. As compared to the control run where $X_o = X_{\text{cntl}} = \sqrt{5\sigma r/2}$ is used, three different initial values of X_o, $0.25X_{\text{cntl}}$, $0.5X_{\text{cntl}}$, or $4X_{\text{cntl}}$, are used in the parallel runs. Since the points are either close to or far from the origin, a saddle point in association with the heating term (rX), these parallel runs help illustrate the impact of the saddle point on solutions. Linear and nonlinear simulations for the parallel and control runs are provided in Fig. 5. As discussed earlier, the trajectories for the primary modes appear as bicycle tubes [e.g. Figs. 5(a)–5(c)], because the corresponding low-frequency components play a dominant role in the solutions. Trajectories with the secondary modes can better reveal the quasi-periodicity [e.g. Fig. 5(d)]. The nonlinear solution for the run with a small X_o in Fig. 5(b) appears as half of a glasswing butterfly in the 3D

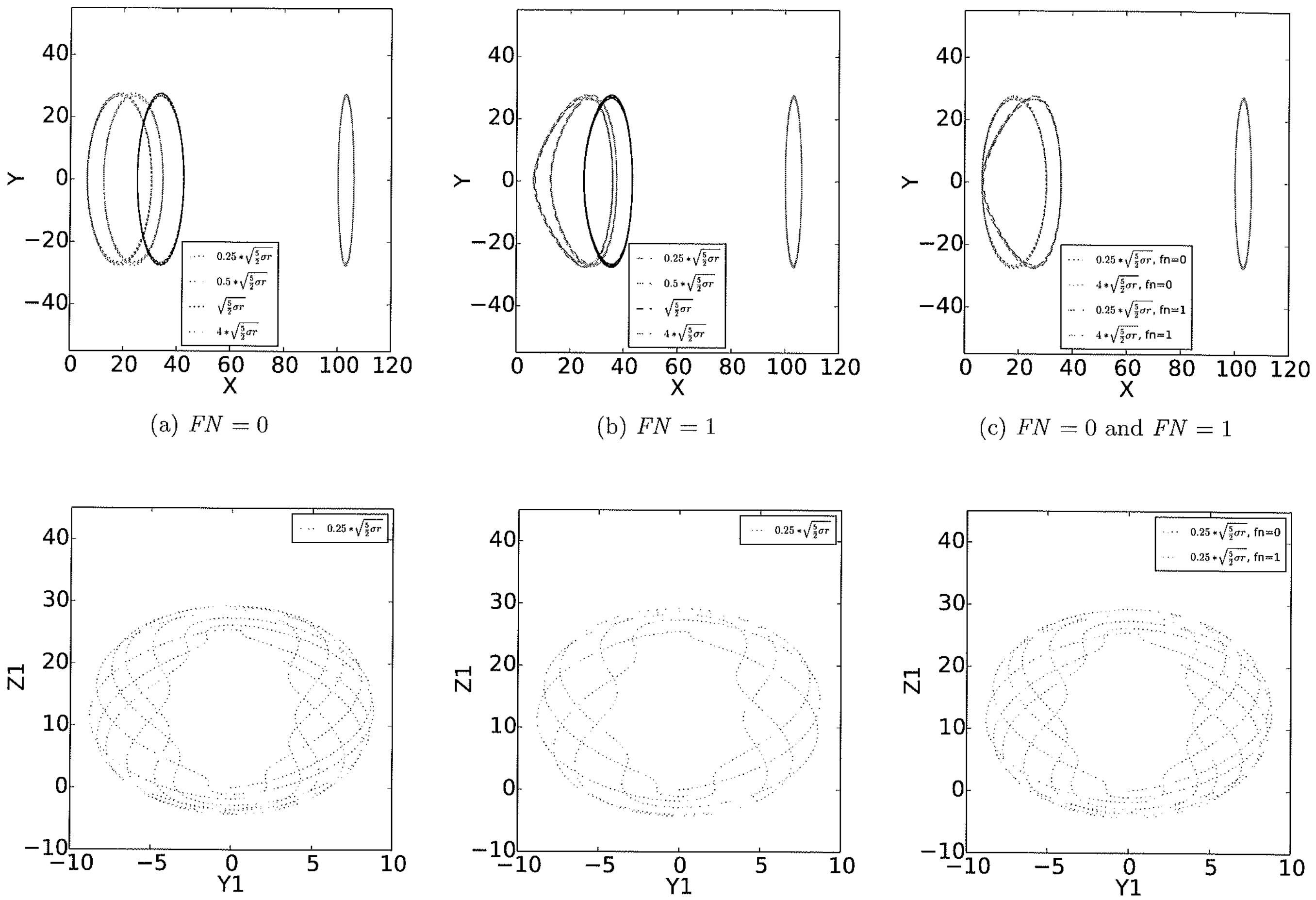

(a) $FN = 0$ (b) $FN = 1$ (c) $FN = 0$ and $FN = 1$

(d) $FN = 0$ (e) $FN = 1$ (f) $FN = 0$ and $FN = 1$

Fig. 5. The impact of various ICs on the solutions. Panels (a)–(b) display X–Y plots from the linear and nonlinear solutions using four different ICs, respectively. Panel (c) displays both linear and nonlinear solutions from two cases for comparison. Panels (d)–(e) display Y_1–Z_1 plots from the linear and nonlinear solutions for the IC of $X_o = 0.25X_{\mathrm{cntl}}$, respectively. Panel (f) includes both of the results from panels (d)–(e).

NLM [e.g. Fig. 9(b) in this study or ~~Fig. 4~~ of [Shen, ~~2017b]~~], indicating the impact of the saddle point. Differences between the linear and nonlinear solutions are clear in Fig. 5(c) and become smaller when initial conditions are further away from the saddle point (i.e. the origin). The same initial conditions are used to perform simulations with the 5D-NLM V1 and the 5D-NLM V2 with $FN = 1$ in order to further verify the results and obtain the same solutions from V1 and V2 with $FN = 1$. As discussed in Sec. 2, the 5D-NLM V2 with $FN = 0$ or $FN = 1$ includes the extended nonlinear feedback loop associated with additional upscaling and downscaling processes. When linear and nonlinear solutions are very close under the condition of a larger X_o, yielding a larger X_c, departures from the reference state (i.e. perturbations) are small. An additional spectrum analysis is provided below.

Figure 6 displays a spectral analysis of the secondary modes for the linear and nonlinear solutions from two runs with initial conditions of $X_o = 0.25X_{\mathrm{cntl}}$ and $X_o = 4X_{\mathrm{cntl}}$. When the initial condition is closer to the saddle point, larger differences between the linear and nonlinear simulations appear [e.g. Fig. 5(c)]. The result is also indicated by more than two peaks in the spectrum of the nonlinear solutions [e.g. Figs. 6(a) and 6(b)]. When the initial condition is far from the saddle point, the locally linear system produces a solution that is a good approximate solution for the nonlinear system [e.g. Figs. 6(c) and 6(d)]. The results above suggest that when X_o is very large and thus is far from the saddle

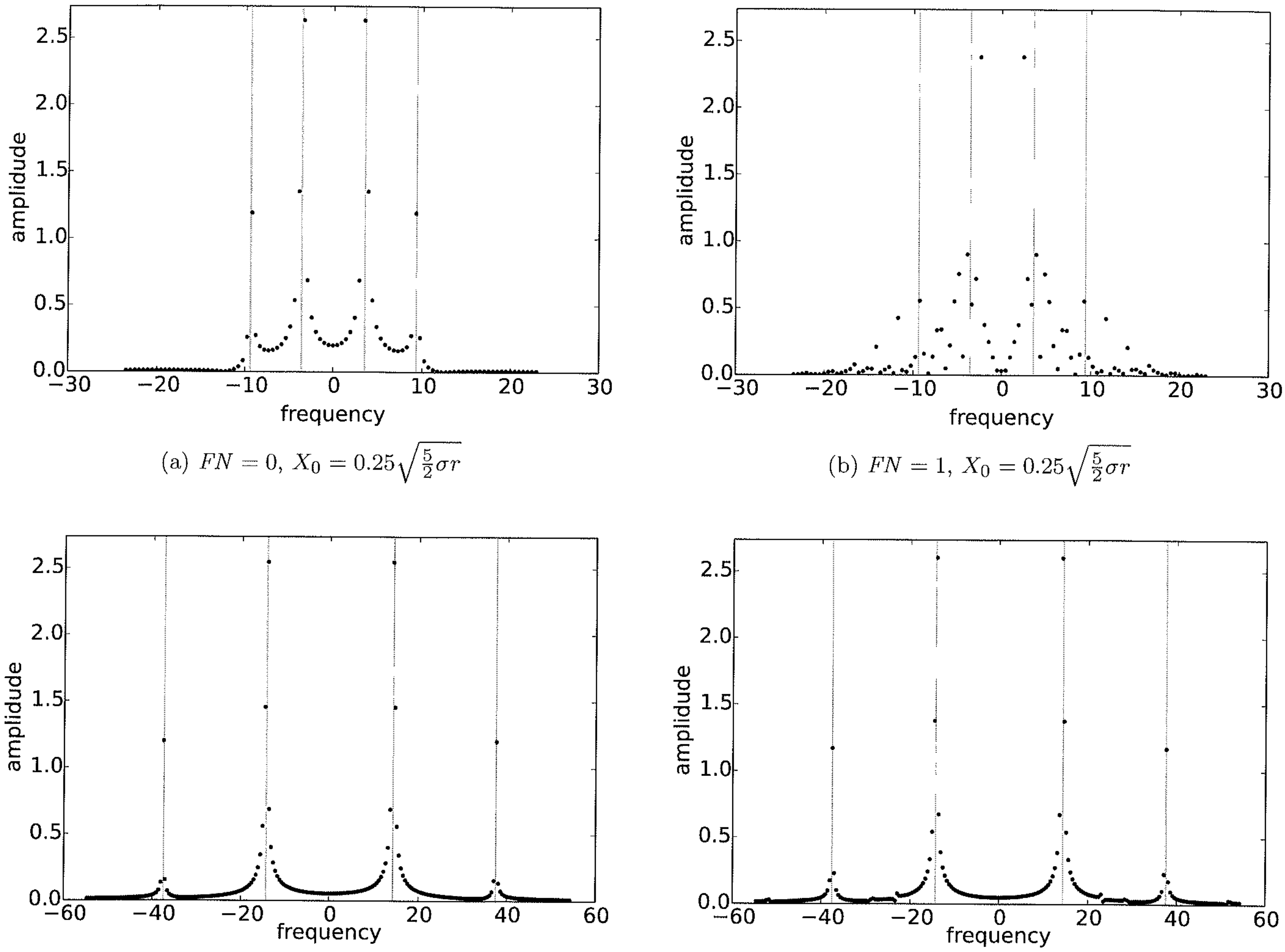

(a) $FN = 0$, $X_0 = 0.25\sqrt{\frac{5}{2}\sigma r}$

(b) $FN = 1$, $X_0 = 0.25\sqrt{\frac{5}{2}\sigma r}$

(c) $FN = 0$, $X_0 = 4\sqrt{\frac{5}{2}\sigma r}$

(d) $FN = 1$, $X_0 = 4\sqrt{\frac{5}{2}\sigma r}$

Fig. 6. A frequency analysis showing the amplitudes of Y_1 at different frequencies, representing the square root of the spectra, from numerical solutions with $X_0 = 0.25\sqrt{\frac{5}{2}\sigma r}$ (top) and $X_0 = 4\sqrt{\frac{5}{2}\sigma r}$ (bottom). Panels (a) and (c) are from linear simulations and panels (b) and (d) are from nonlinear simulations.

point, the nonlinear solution can be approximated by a corresponding linear solution that is quasi-periodic with two incommensurate frequencies.

3.3. *Impact of coupling terms on quasi-periodic solutions*

Stability of the (locally linear) 5D-NLM was previously analyzed using the 5×5 matrix in Eq. (12) that has two pairs of imaginary eigenvalues, leading to two incommensurate frequencies. Here, we further discuss the association of incommensurate frequencies with the extended nonlinear feedback loop. As shown in Eq. (12), the 3×3 submatrix highlighted in the upper box represents the locally linear 3D-NLM (see details in Appendix A). Since the submatrix has eigenvalues 0 and $\pm iX_c$, the (locally linear) system produces an oscillatory solution with a frequency of X_c. In other words, the locally linear version of Eqs. (6)–(8) without inclusion of the feedback term associated with the secondary mode (X_cY_1') is reduced to become the 3D NLM and only has a frequency of X_c. In comparison, the locally linear system in Eqs. (9) and (10) describes the time evolution of the secondary modes (Y_1 and Z_1). When the "control" term associated with the primary mode (X_cZ') is neglected in Eq. (9), the linear subsystem [Eqs. (9) and (10)] is decoupled from the subsystem for the primary modes. The decoupled subsystem can be analyzed using a 2×2 submatrix in the lower box of Eq. (12), as discussed below. Since the submatrix has a pair of imaginary eigenvalues ($\pm i2X_c$), the decoupled subsystem has a periodic solution with a frequency of $2X_c$ that is larger than the solution for the primary mode in the 3D-NLM. Thus, the above matrix analysis without the coupling terms suggests that when the two subsystems for motions of the primary and secondary modes are decoupled, only periodic solutions are observed. This can be also shown ~~with~~ the ~~un~~coupled spring systems ~~as discussed~~ in Appendix C. Thus, all the results indicate the importance of coupling terms in producing quasi-periodic solutions. To illustrate this feature, we further perform simulations using the 5D-NLM V2 with or without the coupling terms, X_cY_1' and X_cZ'. Figure 7 provides the numerical simulations which contain two coupling terms in panel (a), one coupling term (X_cY_1') in panel (b), one coupling term (X_cZ') in panel (c), and no coupling terms in panel (d). As is clear in Fig. 7, only the simulation with two coupling terms displays a quasi-periodic solution. The three additional cases produce a closed orbit.

The discussions provided above using the matrix analysis and model simulations are briefly summarized as follows: (1) Each of the above subsystems that ~~have~~ a frequency of X_c or $2X_c$ is analogous to a single spring system with a spring constant of X_c^2 or $(2X_c)^2$ (also see Appendix C for ~~details~~) and has a periodic solution. (2) The locally linear 3D-NLM is similar to a single spring system. The locally linear 5D-NLM is identical to the system with two coupled springs and two different spring constants that lead to two incommensurate frequencies (as discussed in Appendix C). (3) While the locally linear 3D-NLM has a periodic solution, the locally linear 5D-NLM produces a quasi-periodic solution. (4) The 5D-NLM is derived based on the extension of the nonlinear feedback loop of the 3D-NLM. Both the inclusion of the secondary modes and their coupling with the original primary modes are important for the appearance of the quasi-periodic solutions. (5) The results indicate the dependence of quasi-periodicity on

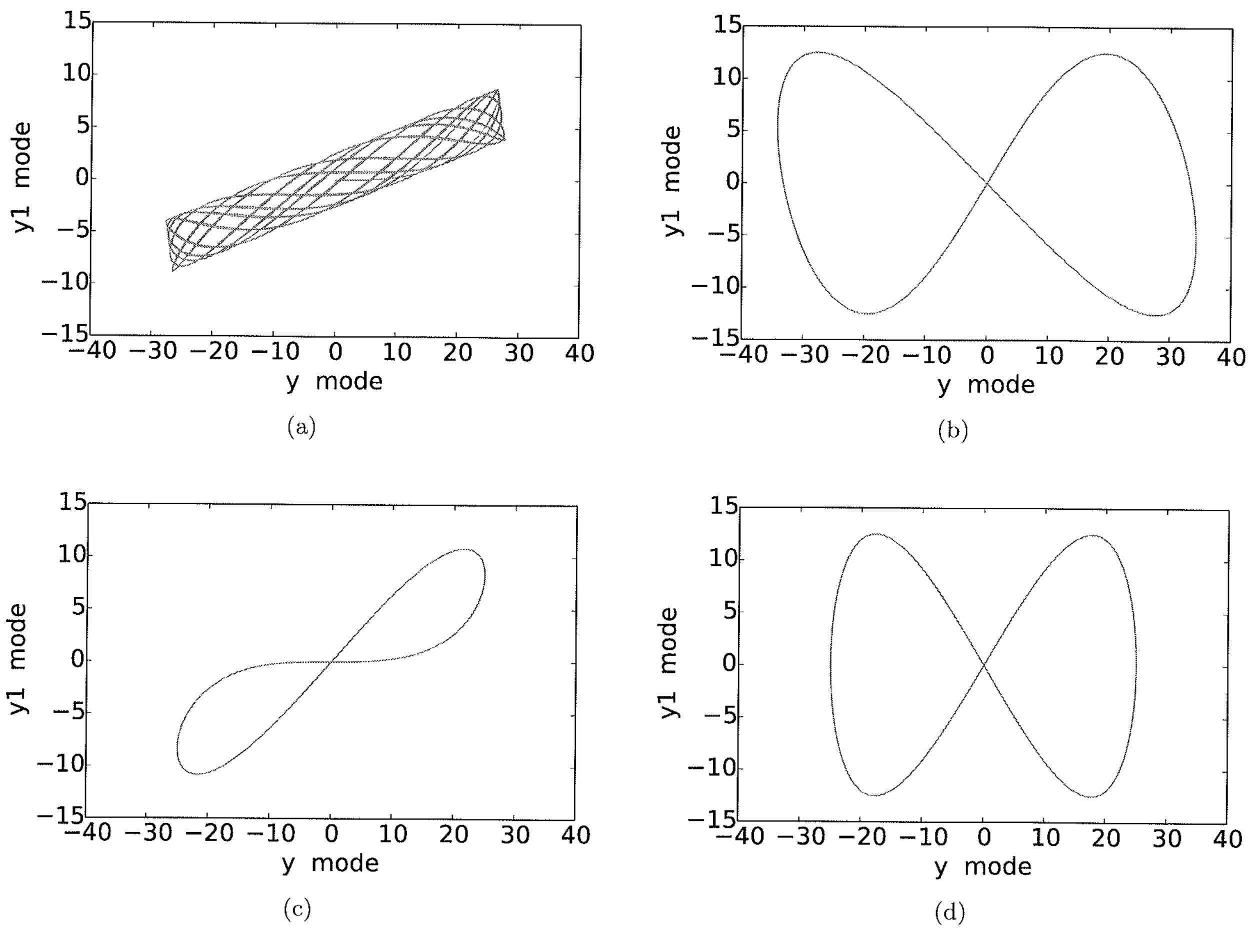

Fig. 7. Solution of LL 5D-NLM $FN = 0$ becomes periodic, if coupling terms XY_1 in $\frac{dZ'}{d\tau}$ and/or XZ in $\frac{dY_1'}{d\tau}$ are ignored. (a) All terms retained for completely coupling, (b) X_cZ' ignored, (c) X_cY_1' ignored and (d) X_cZ' and X_cY_1' ignored.

mode truncation in high-dimensional nondissipative Lorenz models.

4. Concluding Remarks

In this study, we extended our recent work with the 3D-NLM to illustrate the role of the extended nonlinear feedback loop in producing quasi-periodic trajectories using a five-dimensional nondissipative Lorenz model (5D-NLM). Linear analytical solutions were first presented to show two incommensurate frequencies whose ratio is irrational. Linear and nonlinear numerical solutions using the 5D-NLM V2 were presented to illustrate the role of the extended nonlinear feedback loop in producing two incommensurate frequencies; results suggest the dependence of solution's recurrence (e.g. quasi-periodicity) on model coupling (e.g. via a two-way or one-way coupling).

By linearizing the 3D-NLM with respect to a nontrivial critical point, we showed that the feedback loop produces periodic modes. We applied the same method for analyzing the 5D-NLM. As discussed in our previous study, the secondary modes (Y_1 and Z_1) of the 5D-NLM (or its dissipative version) were selected for extending the nonlinear feedback loop of the 3D-NLM and providing a second pair of downscaling (XZ) and upscaling (XY_1) processes. Based on a linear analysis, the 3D-NLM was determined to have one frequency, leading to a periodic solution. The 5D-NLM was determined to have two incommensurate frequencies that yield a quasi-periodic solution. We showed that the occurrence of incommensurate frequencies in the 5D-NLM is associated with the coupling terms (X_cZ' and $X_cY'_1$) that extend the nonlinear feedback loop to provide two-way interactions between the primary (X, Y, Z) and secondary Fourier modes (Y_1, Z_1). The individual impact of the two coupling terms (X_cZ' and $X_cY'_1$) was examined using the so-called one-way interaction approach that disables either the downscaling or upscaling process. A system with one-way interaction always produces periodic solutions with two frequencies whose ratio is rational. A system that decouples the primary and secondary modes by neglecting both of the coupling terms also produces periodic solutions, as expected. A mathematical analogy between the locally linear 5D-NLM and the coupled spring system is provided to illustrate the appearance of the quasi-periodic solution. When an initial condition is far from the saddle point, nonlinear solutions display two prominent frequencies that are similar to those obtained using the linear eigenvalue analysis.

Therefore, we conclude that the extended nonlinear feedback loop within the 5D-NLM leads to the appearance of quasi-periodic solutions that pose challenges for accurately predicting the evolution of solutions (in both magnitudes and phases) when the initial condition displays an uncertainty. In a recent study, we show that a 7D nondissipative LM with further extension of the nonlinear feedback loop can produce three incommensurate frequencies [Shen & Faghih-Naini, 2017]. Since the extension of the nonlinear feedback loop results from spatial mode-mode interactions that are rooted in nonlinear temperature advection, the two studies suggest that quasi-periodic solutions may also appear in higher-dimensional LMs.

One of the original goals was indeed to understand why a high-resolution global model (e.g. [Shen *et al.*, 2006]) with increased degree of nonlinearity can have improved forecasting skills, given the well-accepted view that the source of chaos is nonlinearity. While our idealized Lorenz models still have very limited degree of nonlinearity, as compared to the global model, we have already applied the high-dimensional Lorenz models to address the following weather-related questions: (1) whether an increased degree of nonlinearity always reduces system stability; (2) whether the statement of weather is chaotic is precise; (3) in addition to chaos and (pure) periodicity, does the weather include any other types of solutions? More importantly, we have started applying the dynamics of limit cycle/torus solutions to examine the relationship between the remarkable predictability of African Easterly Waves (e.g. [Shen *et al.*, 2010~~b~~]) and strong surface heating in 30-days simulations. Note that (1) has been partially addressed in our recent studies using high-dimensional Lorenz models; (2)–(3) were discussed at the conferences (e.g. [Shen *et al.*, 2018]); and (4) will be presented at the Asia Oceania Geosciences Society (AOGS) Annual Meeting in June 2018 (e.g. [Shen, ~~2018~~]).

Acknowledgments

We thank anonymous reviewers for valuable comments. We are grateful for support from the College of Science at San Diego State University. Resources supporting this work were provided by the NASA

High-End Computing (HEC) Program through the NASA Advanced Supercomputing (NAS) Division at Ames Research Center.

References

Anthes, R. [2011] "Turning the tables on chaos: Is the atmosphere more predictable than we assume?" UCAR Magazine, spring/summer, available at: https://www2.ucar.edu/atmosnews/opinion/turning-tables-chaos-atmosphere-more-predictable-we-assume-0 (last access: 3 January 2016).

Blender, R. & Lucarini, V. [2013] "Nambu representation of an extended Lorenz model with viscous heating," *Physica D* **243**, 86–91.

Curry, J. H. [1978] "Generalized Lorenz systems," *Commun. Math. Phys.* **60**, 193–204.

Curry, J. H., Herring, J. R., Loncaric, J. & Orszag, S. A. [1984] "Order and disorder in two- and three-dimensional Benard convection," *J. Fluid Mech.* **147**, 1–38.

Fay, T. H. & Graham, S. D. [2003] "Coupled spring equations," *Int. J. Math. Educ. Sci. Technol.* **34**, 65–79.

Felício, C. C. & Rech, P. C. [2018] "On the dynamics of five- and six-dimensional Lorenz models," *J. Phys. Commun.* **2**, 025028.

Floratos, E. [2012] "Matrix quantization of turbulence," *Int. J. Bifurcation and Chaos* **22**, 1250213.

Gleick, J. [1987] *Chaos: Making a New Science* (Penguin, NY), 360 pp.

Hermiz, K. B., Guzdar, P. N. & Finn, J. M. [1995] "Improved low-order model for shear flow driven by Rayleigh–Benard convection," *Phys. Rev. E* **51**, 325–331.

Hirsch, M., Smale, S. & Devaney, R. L. [2013] *Differential Equations, Dynamical Systems, and an Introduction to Chaos*, 3rd edition (Academic Press), 432 pp.

Howard, L. N. & Krishnamurti, R. K. [1986] "Large-scale flow in turbulent convection: A mathematical model," *J. Fluid Mech.* **170**, 385–410.

Jordan, D. W. & Smith, P. [2007] *Nonlinear Ordinary Differential Equations. An Introduction for Scientists and Engineers*, 4th edition (Oxford University Press, NY), 560 pp.

Kreyszig, E [2011] *Advanced Engineering Mathematics*, 10th edition (John Wiley & Sons, ~~Inc~~), 1113 pp.

Lorenz, E. [1963] "Deterministic nonperiodic flow," *J. Atmos. Sci.* **20**, 130–141.

Moon, S., Han, B.-S., Park, J., Seo, J. M. & Baik, J.-J. [2017] "Periodicity and chaos of high-order Lorenz systems," *Int. J. Bifurcation and Chaos* **27**, 1750176-1–11.

Musielak, Z. E., Musielak, D. E. & Kennamer, K. S. [2005] "The onset of chaos in nonlinear dynamical systems determined with a new fractal technique," *Fractals* **13**, 19–31.

Nambu, Y. [1973] "Generalized Hamiltonian dynamics," *Phys. Rev. D* **7**, 2403.

Nevir, P. & Blender, R. [1994] "Hamiltonian and Nambu representation of the non-dissipative Lorenz equations," *Beitraege zur Physik der Atmosphaere* **67**, 133–140.

Roupas, Z. [2012] "Phase space geometry and chaotic attractors in dissipative Nambu mechanics," *J. Phys. A — Math. Theor.* **45**, 195101.

Roy, D. & Musielak, Z. E. [2007a] "Generalized Lorenz models and their routes to chaos. I. Energy-conserving vertical mode truncations, *Chaos Solit. Fract.* **32**, 1038–1052.

Roy, D. & Musielak, Z. E. [2007b] "Generalized Lorenz models and their routes to chaos. II. Energy-conserving horizontal mode truncations," *Chaos Solit. Fract.* **31**, 747–756.

Roy, D. & Musielak, Z. E. [2007c] "Generalized Lorenz models and their routes to chaos. III. Energy-conserving horizontal and vertical mode truncations," *Chaos Solit. Fract.* **33**, 1064–1070.

Saltzman, B. [1962] "Finite amplitude free convection as an initial value problem," *J. Atmos. Sci.* **19**, 329–341.

Shen, B.-W., Atlas, R., Reale, O., Lin, S.-J., Chern, J.-D., Chang, J., Henze, C. & Li, J.-L. [2006] "Hurricane forecasts with a global mesoscale-resolving model: Preliminary results with hurricane Katrina (2005)," *Geophys. Res. Lett.* **33**.

Shen, B.-W., Tao, W.-K., Lau, W. & Atlas, R. [2010~~a~~] "Predicting tropical cyclogenesis with a global mesoscale model: Hierarchical multiscale interactions during the formation of tropical cyclone Nargis (2008)," *J. Geophys. Res.* **115**, D14102.

Shen, B.-W., Tao, W.-K. & Wu, M.-L. [2010~~b~~] "African easterly waves in 30-day high-resolution global simulations: A case study during the 2006 NAMMA period," *Geophys. Res. Lett.* **37**, L18803.

Shen, B.-W., DeMaria, M., Li, J.-L. F. & Cheung, S. [2013] "Genesis of hurricane sandy (2012) simulated with a global mesoscale model," *Geophys. Res. Lett.* **40**.

Shen, B.-W. [2014] "Nonlinear feedback in a five-dimensional Lorenz model," *J. Atmos. Sci.* **71**, 1701–1723.

Shen, B.-W. [2015] "Nonlinear feedback in a six-dimensional Lorenz model. Impact of an additional heating term," *Nonlin. Process. Geophys.* **22**, 749–764.

Shen, B.-W. [2016] "Hierarchical scale dependence associated with the extension of the nonlinear feedback loop in a seven-dimensional Lorenz model," *Nonlin. Process. Geophys.* **23**, 189–203.

Shen, B.-W. & Faghih-Naini, S. [2017] "On recurrent solutions in high-dimensional non-dissipative Lorenz models," *The 10th Chaos Modeling and Simulation Int. Conf. (CHAOS2017)*, Barcelona, Spain.

Shen, B.-W. [2017a] "On an extension of the nonlinear feedback loop in a nine-dimensional Lorenz model," *Chaotic Model. Simul.* (*CMSIM*) **2**, 147–157.

Shen, B.-W. [2017b] "On periodic solutions in the non-dissipative Lorenz model: The role of the nonlinear feedback loop," ~~(submitted to Tellus — A for publication, November, 2017).~~

Shen, B.-W. [2018] "Understanding the predictability of short-term climate simulations of African easterly waves using a global mesoscale model and idealized Lorenz model," *AOGS 15th Annual Meeting*, Honolulu, Hawaii.

Shen, B.-W., Pielke Sr., R. A., Zeng, X., Santos, I. A., Faghih-Naini, S., Buchmann, J., Shie, C.-J. & Atlas, R. [2018] "Butterfly effects of the first and second kinds in Lorenz models," AMS 2018 annual meeting. Presentation slides are available as a google document from https://goo.gl/hbxRgE

Solomon, S., Qin, D., Manning, M., Chen, Z., Marquis, M., Averyt, K., Tignor, M. & Miller Jr., H. L. (eds.) [2007] *Climate Change 2007: The Physical Science Basis* (Cambridge University Press), 996 pp.

Sprott, J. C. [2003] *Chaos and Time-Series Analysis* (Oxford University Press), 528 pp. The numerical method is briefly discussed on http://sprott.physics.wisc.edu/chaos/lyapexp.htm.

Strogatz, S. H. [2015] *Nonlinear Dynamics and Chaos. With Applications to Physics, Biology, Chemistry, and Engineering* (Westpress View, Boulder, CO), 513 pp.

Thiffeault, J.-L. & Horton, W. [1996] "Energy-conserving truncations for convection with shear flow," *Phys. Fluids* **8**, 1715–1719.

Thompson, J. M. T. & Stewart, H. B. [2002] *Nonlinear Dynamics and Chaos*, 2nd edition (John Wiley & Sons), 437 pp.

Appendices

Appendix A

Linear Analytical Solutions for the 3D-NLM

In this Appendix, we verify our numerical approaches by comparing the numerical solutions of the locally linear 3D-NLM with the analytical solutions. We then illustrate the impact of nonlinearity by comparing the linear and nonlinear numerical solutions. When the terms that include secondary modes (i.e. Y_1) are neglected, Eqs. (6)–(8) are reduced to become:

$$\frac{dX'}{d\tau} = \sigma Y', \tag{A.1}$$

$$\frac{dY'}{d\tau} = (r - Z_c)X' - X_c Z' - FN(X'Z'), \tag{A.2}$$

$$\frac{dZ'}{d\tau} = Y_c X' + X_c Y' + FN(X'Y'). \tag{A.3}$$

The locally linear system with $FN = 0$ yields the following equation:

$$\frac{d\overrightarrow{U'}}{d\tau} = A^{3D}\overrightarrow{U'}, \tag{A.4}$$

$$A^{3D} = \begin{pmatrix} 0 & \sigma & 0 \\ 0 & 0 & -X_c \\ 0 & X_c & 0 \end{pmatrix}. \tag{A.5}$$

The transpose of $\overrightarrow{U'}$ is (X', Y', Z'). The above matrix has the following three eigenvalues: 0, iX_c, and $-iX_c$, as well as their corresponding eigenvectors:

$$\overrightarrow{V_1} = \begin{pmatrix} 1 \\ 0 \\ 0 \end{pmatrix}, \quad \overrightarrow{V_2} = \begin{pmatrix} \dfrac{\sigma}{X_c} \\ i \\ 1 \end{pmatrix}, \quad \overrightarrow{V_3} = \begin{pmatrix} \dfrac{\sigma}{X_c} \\ -i \\ 1 \end{pmatrix}. \tag{A.6}$$

Using the above eigenvectors as the basis functions, a general solution is written as follows:

$$\overrightarrow{U'}(\tau) = C_1 e^{\lambda_1 \tau}\overrightarrow{V_1} + C_2 e^{\lambda_2 \tau}\overrightarrow{V_2} + C_3 e^{\lambda_3 \tau}\overrightarrow{V_3}, \tag{A.7}$$

which leads to

$$\begin{pmatrix} X' \\ Y' \\ Z' \end{pmatrix} = C_1 \begin{pmatrix} 1 \\ 0 \\ 0 \end{pmatrix} + (C_2 + C_3) \begin{pmatrix} \dfrac{\sigma}{X_c}\cos(X_c\tau) \\ -\sin(X_c\tau) \\ \cos(X_c\tau) \end{pmatrix} + i(C_2 - C_3) \begin{pmatrix} \dfrac{\sigma}{X_c}\sin(X_c\tau) \\ \cos(X_c\tau) \\ \sin(X_c\tau) \end{pmatrix}. \tag{A.8}$$

Here, C_1, C_2, and C_3 can be determined by an IC at $\tau = 0$. Given an IC $(X, Y, Z) = (X_0, 0, 0)$, we have $(X', Y', Z') = (X_o - X_c, -Y_c, -Z_c)$ with $Z_c = r$ and $Y_c = 0$. Furthermore, $X_c = \sqrt{2\sigma r + X_0^2}$ as a result of the relationship derived from the conservation law $X^2/2 - \sigma(Z) = X_o^2/2$. Without a loss of generality, $X_0 = \sqrt{2\sigma r}$ is chosen for the control run and

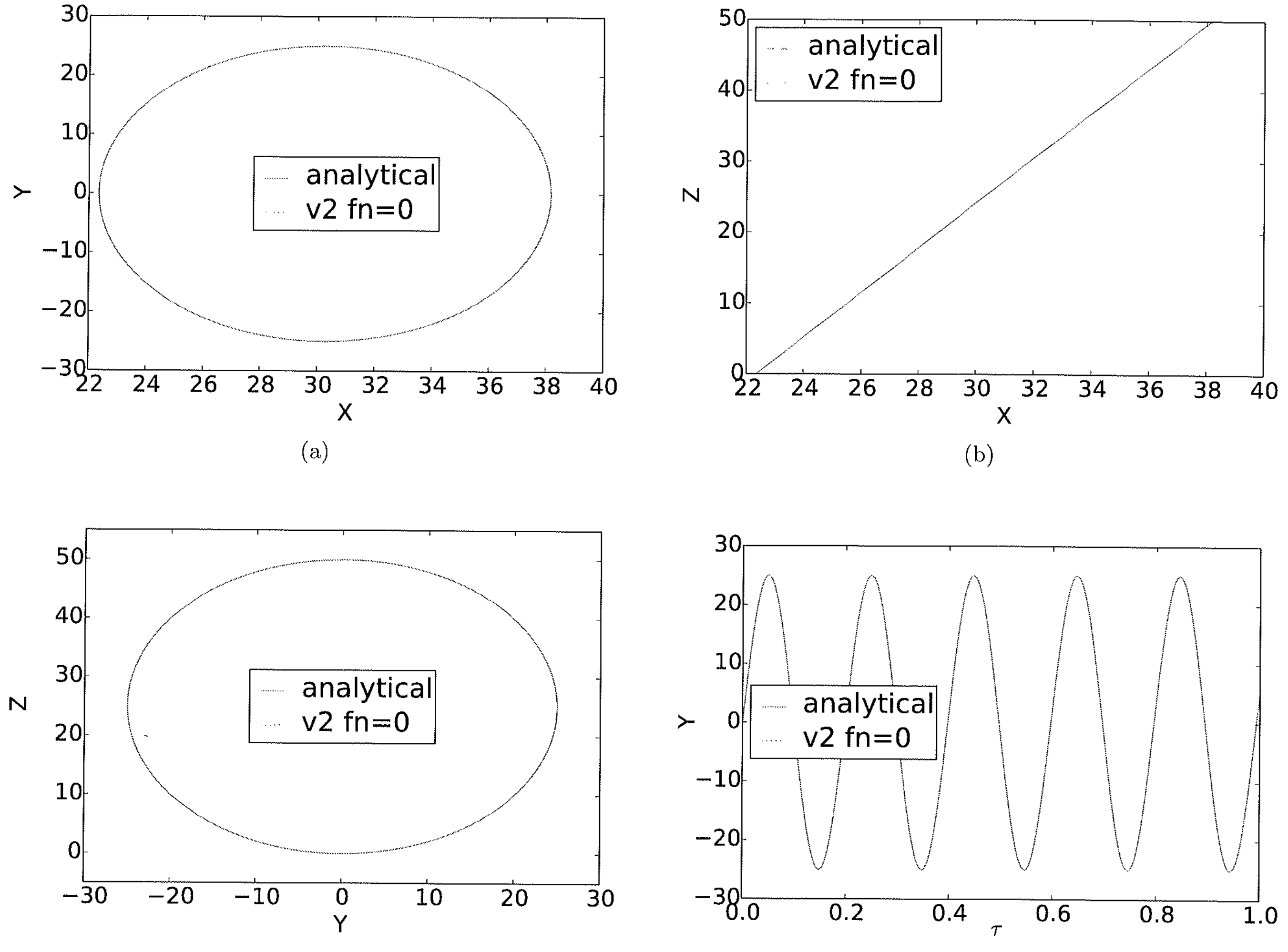

(a) (b) (c) (d)

Fig. 8. A comparison of analytical and numerical solutions from the locally linear 3D-NLM. (a) X–Y, (b) X–Z, (c) Y–Z and (d) τ–Y.

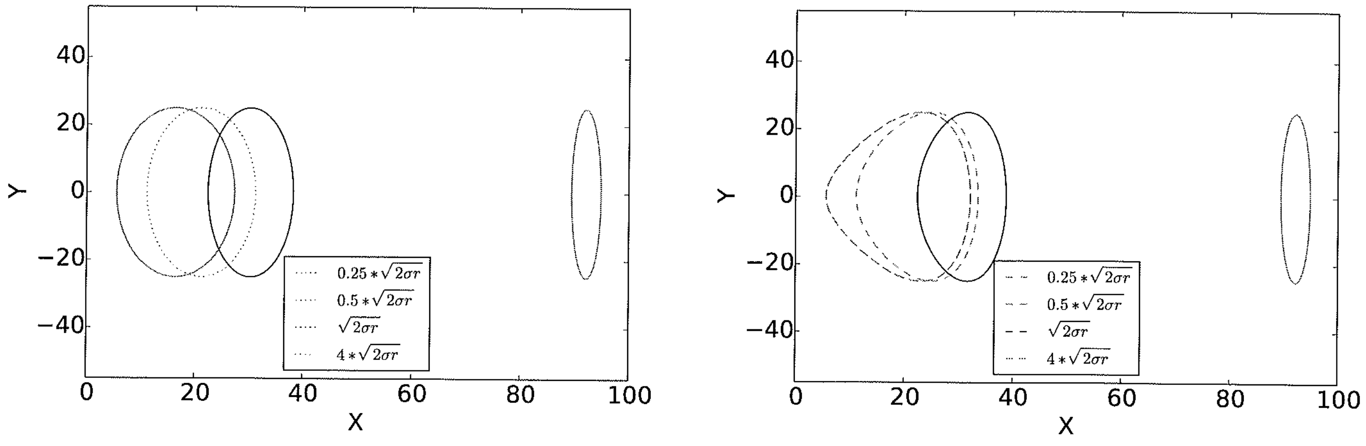

(a) $FN = 0$ (b) $FN = 1$

Fig. 9. The impact of various ICs on solutions of the 3D-NLM V2. Panels (a)–(b) display X–Y plots for linear and nonlinear solutions, respectively. Panel (c) provides both linear and nonlinear results from two cases. Panel (d) displays the time evolution of Y for linear and nonlinear simulations from two runs with different ICs.

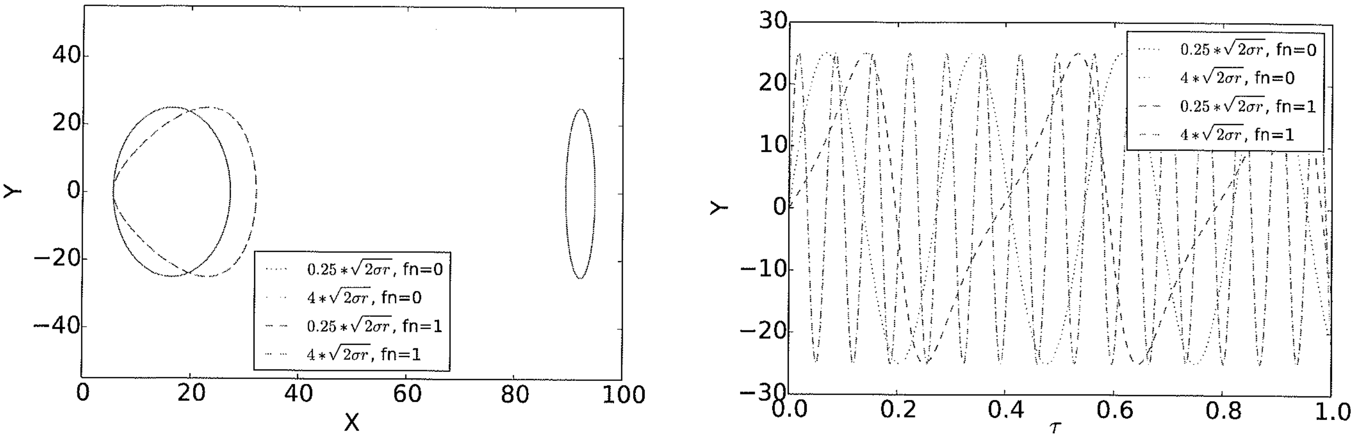

(c) $FN = 0$ and $FN = 1$

(d) $FN = 0$ and $FN = 1$

Fig. 9. (*Continued*)

X_0 is varied in parallel runs. Applying the above IC in Eq. (A.8), we have

$$\begin{pmatrix} X_o - X_c \\ 0 \\ -r \end{pmatrix} = C_1 \begin{pmatrix} 1 \\ 0 \\ 0 \end{pmatrix} + (C_2 + C_3) \begin{pmatrix} \dfrac{\sigma}{X_c} \\ 0 \\ 1 \end{pmatrix} + i(C_2 - C_3) \begin{pmatrix} 0 \\ 1 \\ 0 \end{pmatrix}. \tag{A.9}$$

While the second row (component) of Eq. (A.9) leads to $C_2 = C_3$, the third row yields $C_2 + C_3 = -r$. Thus, $C_2 = C_3 = -r/2$. Plugging C_2 and C_3 into the first row of Eq. (A.9), we obtain $C_1 = X_o - X_c + \frac{\sigma r}{X_c} = \frac{(2\sqrt{2}-3)\sqrt{\sigma r}}{2}$. For $\sigma = 10$ and $r = 25$, $C_1 \approx -1.3564$ and $C_2 = C_3 = -12.5$.

Figure 8 displays the analytical solution and the linear numerical solutions from Eqs. (A.1)–(A.3) with $FN = 0$, indicating good agreement between them. Figure 9 compares linear and nonlinear solutions with various initial conditions. The nonlinear solutions were previously studied by Shen [2017b]. As shown in Figs. 9(c) and 9(d), differences between the linear and nonlinear solutions are significant when the initial condition is closer to the origin (i.e. the saddle point).

Appendix B

Derivations of Linear Analytical Solutions for the 5D-NLM

Appendix B discusses how the coefficients C_1–C_5 in Eq. (21) are determined to obtain the solution in Eq. (22). To facilitate discussions, we define the following time-independent parameters: $A_1 = \frac{-\beta_1^2}{2X_c^3} + \frac{5}{2X_c}$, $A_3 = \frac{-\beta_3^2}{2X_c^3} + \frac{5}{2X_c}$, $M = C_1 + C_2$, $N = i(C_1 - C_2)$, $P = C_3 + C_4$ and $Q = i(C_3 \quad C_4)$. By plugging the above into Eqs. (18) and (21), we have:

$$\begin{pmatrix} X' \\ Y' \\ Z' \\ Y_1' \\ Z_1' \end{pmatrix} = M \begin{pmatrix} \sigma A_1 \cos(\beta_1 \tau) \\ -\beta_1 A_1 \sin(\beta_1 \tau) \\ \left(\dfrac{-\beta_1^2}{2X_c^2} + 2\right) \cos(\beta_1 \tau) \\ \dfrac{-\beta_1}{2X_c} \sin(\beta_1 \tau) \\ \cos(\beta_1 \tau) \end{pmatrix} + N \begin{pmatrix} \sigma A_1 \sin(\beta_1 \tau) \\ \beta_1 A_1 \cos(\beta_1 \tau) \\ \left(\dfrac{-\beta_1^2}{2X_c^2} + 2\right) \sin(\beta_1 \tau) \\ \dfrac{\beta_1}{2X_c} \cos(\beta_1 \tau) \\ \sin(\beta_1 \tau) \end{pmatrix} + P \begin{pmatrix} \sigma A_3 \cos(\beta_3 \tau) \\ -\beta_3 A_3 \sin(\beta_3 \tau) \\ \left(\dfrac{-\beta_3^2}{2X_c^2} + 2\right) \cos(\beta_3 \tau) \\ \dfrac{-\beta_3}{2X_c} \sin(\beta_3 \tau) \\ \cos(\beta_3 \tau) \end{pmatrix}$$

$$+Q\begin{pmatrix}\sigma A_3\sin(\beta_3\tau)\\ \beta_3A_3\cos(\beta_3\tau)\\ \left(\frac{-\beta_3^2}{2X_c^2}+2\right)\sin(\beta_3\tau)\\ \frac{\beta_3}{2X_c}\cos(\beta_3\tau)\\ \sin(\beta_3\tau)\end{pmatrix}$$

$$+C_5\begin{pmatrix}\sigma\\0\\0\\0\\0\end{pmatrix}. \tag{B.1}$$

Applying the initial condition at $\tau = 0$, we obtain:

$$\begin{pmatrix}X_o-X_c\\0\\-r\\0\\-\frac{r}{2}\end{pmatrix} = M\begin{pmatrix}\sigma A_1\\0\\ \frac{-\beta_1^2}{2X_c^2}+2\\0\\1\end{pmatrix} + N\begin{pmatrix}0\\ \beta_1A_1\\0\\ \frac{\beta_1}{2X_c}\\0\end{pmatrix}$$

$$+P\begin{pmatrix}\sigma A_3\\0\\ \frac{-\beta_3^2}{2X_c^2}+2\\0\\1\end{pmatrix} + Q\begin{pmatrix}0\\ \beta_3A_3\\0\\ \frac{\beta_3}{2X_c}\\0\end{pmatrix}$$

$$+C_5\begin{pmatrix}\sigma\\0\\0\\0\\0\end{pmatrix}. \tag{B.2}$$

From the second and fourth rows (or components), we have:

$$\beta_1A_1N + \beta_3A_3Q = 0, \tag{B.3}$$

$$\frac{\beta_1}{2X_c}N + \frac{\beta_3}{2X_c}Q = 0, \tag{B.4}$$

yielding $N = Q = 0$ as the result of $\beta_1 \neq \beta_3$ and $A_1 \neq A_3$. Thus, we have $C_1 = C_2$ and $C_3 = C_4$. The first, third, and fifth rows give the following equations, respectively:

$$A_1M + A_3P + C_5 = \frac{X_0 - X_c}{\sigma}, \tag{B.5}$$

$$\left(\frac{-\beta_1^2}{2X_c^2}+2\right)M + \left(\frac{-\beta_3^2}{2X_c^2}+2\right)P = -r, \tag{B.6}$$

$$M + P = \frac{-r}{2}. \tag{B.7}$$

Solving the above equations, we have:

$$\begin{gathered}M = \frac{-\beta_3^2 r}{2(\beta_3^2-\beta_1^2)},\quad P = \frac{\beta_1^2 r}{2(\beta_3^2-\beta_1^2)}\quad\text{and}\\ C_5 = \frac{X_0-X_c}{\sigma} + \frac{5r}{4X_c},\end{gathered} \tag{B.8}$$

representing the coefficients of the right-hand sides in Eq. (22), respectively.

Appendix C

An Analogy Between the Locally Linear 5D-NLM and a Coupled Spring System

Using $Y_c = 0$, $Y_{1c} = 0$, $Z_c = r$, $Z_{1c} = \frac{r}{2}$, and $FN = 0$, Eqs. (6)–(10) represent the locally linear

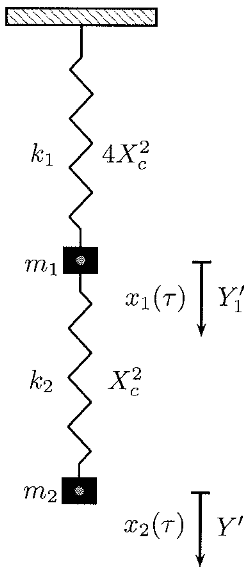

Fig. 10. A coupled system with two springs and two masses with the same weight (i.e. $m_1 = m_2$). k_1 and k_2 are spring constants. $x_1(\tau)$ and $x_2(\tau)$ are the displacements of the centers of masses from equilibrium. When $x_1 = Y_1'$, $k_1 = 4X_c^2$, $x_2 = Y'$, and $k_2 = X_c^2$, the equations of the coupled spring system are identical to those in the locally linear 5D-NLM.

5D-NLM with respect to the nontrivial critical point. From Eqs. (7) and (8), we can obtain:

$$\frac{d^2Y'}{d\tau^2} = -X_c\frac{dZ'}{d\tau} = -X_c(X_cY' - X_cY'_1)$$
$$= -X_c^2(Y' - Y'_1). \tag{C.1}$$

Equations (9) and (10) lead to:

$$\frac{d^2Y'_1}{d\tau^2} = X_c\frac{dZ'}{d\tau} - 2X_c\frac{dZ'_1}{d\tau}$$
$$= X_c(X_cY' - X_cY'_1) - 2X_c(2X_cY'_1)$$
$$= X_c^2Y' - 5X_c^2Y'_1. \tag{C.2}$$

In comparison, by considering a model with two springs and two masses with the same weight, the equations can be written, as follows (e.g. Eq. (2.1) of [Fay & Graham, 2003; Kreyszig, 2011]):

$$\frac{d^2x_1}{d\tau^2} = -k_1x_1 - k_2(x_1 - x_2), \tag{C.3}$$

$$\frac{d^2x_2}{d\tau^2} = -k_2(x_2 - x_1). \tag{C.4}$$

Here, an upper spring with a spring constant k_1 is attached to the ceiling on one end and to the first mass on the other end, as shown in Fig. 10. The upper (low) end of the low spring with a spring constant k_2 is attached to the first (second) mass. $x_1(\tau)$ and $x_2(\tau)$ are the displacements of the centers of masses from equilibrium. Since the first mass experiences two restoring forces from both springs and since the second mass is only influenced by the low spring, we may choose $x_1 = Y'_1$, $k_1 = 4X_c^2$, $x_2 = Y'$, and $k_2 = X_c^2$. Thus, Eqs. (C.3) and (C.4) are identical to Eqs. (C.2) and (C.1), respectively.